analytical chemistry

pubs.acs.org/ac Article

Carbon Nanotube Microelectrode Set: Detection of Biomolecules to Heavy Metals

Pankaj Gupta, Connor E. Rahm, Benjamin Griesmer, and Noe T. Alvarez*

Cite This: *Anal. Chem.* 2021, 93, 7439–7448 Read Online

ACCESS | Metrics & More | Article Recommendations | Supporting Information

ABSTRACT: An ultrasensitive electrochemical microelectrode set (μ-ES), where all three electrodes are made of highly densified carbon nanotube fiber (HD-CNTf) cross sections (length ~40 μm), embedded in an inert polymer matrix, and exposed open-ended CNTs at the interface, is presented here. Bare open ends of HD-CNTf rods were used as the working (~40 μm diameter) and counter (~94 μm diameter) electrodes, while the cross section of a ~94 μm diameter was electroplated with Ag/AgCl and coated with Nafion to employ as a quasi-reference electrode. The Ag/AgCl/Nafion-coated HD-CNTf rod quasi-reference electrode provided a very stable potential comparable to the commercial porous-junction Ag/AgCl reference electrode. The HD-CNTf rod μ-ES has been evaluated by electrochemical determination of biologically important analytes, i.e., dopamine (DA), β-nicotinamide adenine dinucleotide (NADH), a diuretic drug, i.e., furosemide, and a heavy metal, i.e., lead ions (Pb^{2+}). Different voltammetric techniques were employed during the study, i.e., cyclic voltammetry (CV), square wave voltammetry (SWV), amperometry, and square wave anodic stripping voltammetry (SWASV). The direct metallic connection to CNTs gives access to the exceptional properties of highly ordered open-ended CNTs as electrochemical sensors. The distinct structural and electronic properties of aligned HD-CNTf rods in the μ-ES demonstrate fast electron transfer kinetics and offer excellent detection performance during testing for different analytes with wide linear ranges, excellent sensitivity, and very low limits of detection.

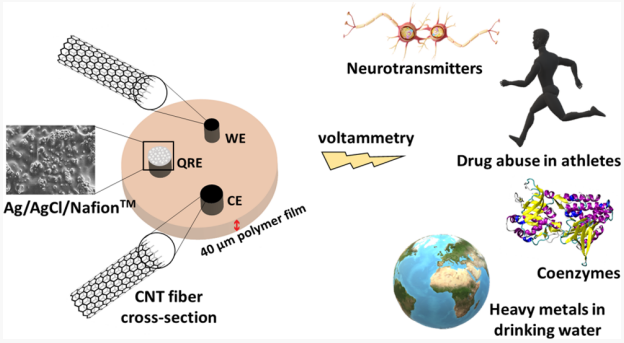

INTRODUCTION

The scientific work on CNTs was greatly boosted after the Iijima reports,[1,2] which projected CNTs onto the global scientific platform. Carbon nanotubes (CNTs) have attracted enormous interest due to their unique electronic and mechanical properties, and identified as an excellent electrode material because of their high aspect ratio, nanometer dimensions, fast electron transfer rate, ample electroactive sites, biocompatibility, and corrosion resistance.[3−9] The conductivity of CNTs, along with their small size, ideally makes them the smallest possible electrode material with a diameter of less than nanometer.[9,10] The first report of CNTs-based electrode was used to study the oxidation of dopamine by voltammetric techniques.[11] Dopamine showed an ideal reversible two-electron redox process which had not been observed previously on graphite or carbon electrodes. The observed results opened up a new world for CNTs use as an electrode material in a wide range of sensing applications.[6,9,12,13] Indeed, a significant growth has been seen over the past two decades in CNT technology, where several papers reported the use of CNTs as randomly dispersed or drop coating on macro carbon (glassy carbon, graphite), Au, Pt surfaces,[8,14,15] dispersions with the assistance of binders,[16−18] pastes,[19−22] screen printed inks,[23−25] CNT papers,[26−28] composites,[29,30] and simple adhesion on electrode surfaces[31,32] for the electrochemical detection of a wide range of redox-active molecules. The reported studies claimed that CNTs-based electrodes were able to reduce overpotential with fast electron transfer kinetics, increased peak current response, high sensitivity, and selectivity to analytes compared to bare electrode surfaces.

Further efforts have also been made to gain better control over distribution, orientation, and alignment of nanotubes by direct growth and self-assembly to exploit the electrochemistry of CNTs.[33−38] Highly ordered CNT fibers and array assemblies take advantage of the bulk properties of CNTs while avoiding dispersion of individual CNTs in the solution. In comparison to randomly arranged CNT-based electrodes, highly ordered or aligned CNT electrodes show high mass sensitivity, faster mass transport, lower solution resistance, and

Received: January 25, 2021
Accepted: May 4, 2021
Published: May 14, 2021

https://doi.org/10.1021/acs.analchem.1c00360
Anal. Chem. 2021, 93, 7439−7448

high signal-to-noise ratio, resulting in much lower background current and improved detection limits.[39,40] The alignment of CNTs within the fiber inherits the advantage of large specific surface area and electrocatalytic activity of CNTs and helps to exploit the anisotropic properties of individual CNTs.[34−36,41−47] The diameter of dry spun CNT fiber can be customized by changing the width of the chemical vapor deposition (CVD)-grown CNT forests and through the mechanical spinning process, i.e., twisting voltage and angle, and thereby CNT fiber can be tailored for use as electrodes to a range of applications.[48−50] The electrochemical sensor based on CNT fibers was first reported by Wang et al.[41] and was spun from wet CNTs for the electrochemical sensing of NADH, peroxide, and dopamine. Later, CNT fiber microelectrodes made using the dry spun process have been reported by Zhu et al.[51] for glucose biosensing, and Heineman et al.[52,53] for heavy metal detection. CNT fiber microelectrodes have also been an ideal material for neural stimulation and long-term selective recording compared to the traditional electrode material.[54,55] CNT fibers are clearly gaining ground as new-generation sensors and an alternative for the conventional carbon fiber microelectrode for more sensitive and selective in vitro and in vivo electrochemical studies of neuronal cells. Also, CNT fibers are superior for real-time monitoring of neurotransmitters and their metabolites in live brain tissues with improved spatiotemporal resolution.[7,47,56−58] The high surface roughness and presence of oxygen functionalities on dangling sp^3-hybridized carbon edge planes of the CNT fiber provide resistance to fouling. Thus, it allows increased sensitivity and reproducibility over a long period of time.[36,46,59−61]

Here, we report the first use of a microelectrode set (μ-ES), where all three electrodes are made of well-aligned highly densified multiwalled carbon nanotube fibers (HD-CNTf) sectioned into rods embedded in an inert polymer film with exposed open ends of CNTs at the electrode−electrolyte interface. Our goal was to fabricate a microstructured and compact sensing device in which all three electrodes are based on CNTs, which is advantageous during fabrication. The sidewalls of the CNTs are encapsulated to take advantage of the unparalleled sensitivity of their open ends. The micro size length and diameter of all three CNT fiber electrodes allow the miniaturization of the entire sensor onto a single platform, where even a single drop of desired analyte solution will be enough for electrochemical characterization. Herein, we have quantitatively characterized the performance of the proposed HD-CNTf rod μ-ES sensor by different voltammetric techniques, i.e., cyclic voltammetry (CV), square wave voltammetry (SWV), amperometry, and square wave anodic stripping voltammetry (SWASV) for the sensitive detection of important biomolecules (dopamine, β-nicotinamide adenine dinucleotide; NADH), diuretic drug (furosemide) in phosphate buffer solution, and heavy metal, i.e., lead (Pb^{2+}) in tap water. The HD-CNTf rod μ-ES showed an excellent range of quantification toward biomolecules and heavy metal determination. The excellent sensitivity of the HD-CNTf rod electrode can be attributed to the presence of a higher number of edge plane sites on the cross section of HD-CNTf per square micrometer.[35,40,62] CNT-coated and CNT fiber electrodes used for the detection of dopamine,[63−65] NADH,[66] furosemide,[67−69] and Pb^{2+}.[53,70,71] The novelty of the technology rests on the μ-ES design, where all three electrodes, based on the CNT rods, were assembled on the same platform and directly connected to a metallic contact for electronic circuits at one side and exposed highly densified open ends on other side being used for testing analytes. Thus, the reported design allows us to exploit the exceptional properties of pure CNTs in the electrochemical sensing of different important biomolecules and an environmentally toxic heavy metal in different electrolyte mediums.

EXPERIMENTAL SECTION

Reagents and Materials. Lead, dopamine (DA), uric acid, ascorbic acid, furosemide, NADH (β-nicotinamide adenine dinucleotide, reduced form), 5% Nafion solution, $[Ru(NH_3)_6]Cl_3$, and KCl were purchased from Sigma-Aldrich. Phosphate buffer of 0.1 M ionic strength was prepared using trace metal salts H_3PO_4, Na_2HPO_4, and NaH_2PO_4 according to the reported method.[72] For the preparation of a CNT fiber cross-section-embedded polymer film, an EMBed-812 embedding kit was purchased from Electron Microscopy Sciences (Pennsylvania) and monomer mixed according to given instructions. Acetone solvent was used for fiber densification. All solutions were prepared in Milli-Q ultrapure deionized water (18 MΩ cm). CNT arrays were synthesized using CVD as reported by our group before,[49,50] where ethylene (Wright Brothers) was used as the carbon source and Fe/Co as the catalyst (Goodfellow).

Instrumentation. An Epsilon EClipse electrochemical analyzer from BASi and a CHI 760E electrochemical workstation from CH instruments were used to record voltammetric experiments. The μ-ES consists of three HD-CNTf rods in which a ∼40 μm diameter HD-CNTf rod is used as the working electrode, while two others ∼94 μm diameter HD-CNTf rods are used as counter and reference electrodes. The reference electrode is coated with Ag/AgCl/Nafion to perform as the quasi-reference electrode. For comparison of the HD-CNTf rod quasi-reference electrode, a Ag/AgCl (3 M NaCl) (ALS Co., Ltd, model 012167 RE-1B) was used as a standard reference electrode. CVs, SWVs, and SWASVs were recorded with an Epsilon EClipse, while amperometry was recorded using the CHI 760E instruments. The surface morphology of HD-CNTf rods was performed using field emission-scanning electron microscopy (FE-SEM) FEI XL30 operated at 10 kV acceleration voltage.

Experimental Procedure. The stock solutions of $[Ru(NH3)_6]Cl_3$ (5 mM), DA (1 mM), NADH (10 mM), and Pb^{2+} (10 000 ppb) were prepared in deionized water, while furosemide (1 mM) was prepared in ethanol. For the electrochemical characterization of the working electrode, CVs were recorded in 1:1 ratio of 5 mM $[Ru(NH_3)_6]Cl_3$ and 50 mM KCl solution. To record the voltammograms of biomolecules, 2 mL of phosphate buffer and the required amount of the desired analyte were added to the electrolytic cell and the total volume was made to 4 mL using DI water. Voltammograms were then recorded under optimized parameters. Optimized square wave voltammetry (SWV) parameters were square wave amplitude: 25 mV, potential step: 4 mV, and square wave frequency (f): 15 Hz. Between the measurement of biomolecules, a 60 s clean step (controlled potential electrolysis; CPE) at 500 mV for DA and NADH and at 1000 mV for furosemide was running. Pb^{2+} was deposited at −1200 mV for 120 s and square wave stripping voltammetry (SWSV) was performed using step potential of 4 mV, frequency (f) of 15 Hz, and amplitude of 25 mV. Between the SWSV measurements, a 120 s CPE at 800 mV was performed to remove any residual heavy metal ions from the

https://doi.org/10.1021/acs.analchem.1c00360
Anal. Chem. 2021, 93, 7439−7448

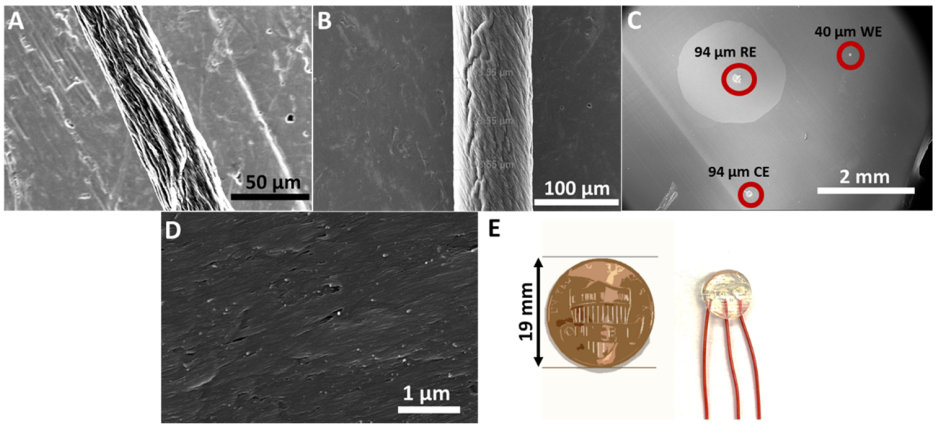

Figure 1. FE-SEM images of (A) ∼40 μm and (B) ∼94 μm HD-CNTf; (C) polymer-embedded cross section of three HD-CNTf rods in red circles used as working, quasi-reference, and counter electrodes, and (D) high magnification image of HD-CNTf rod cross section and (E) optical image of developed HD-CNTf rods as μ-ES for size assessment compare with the US 1 cent coin.

electrode surface. During lead electrodeposition, a magnetic stirrer was used to stir the test solutions. The HD-CNTf rods microsensor was performed in triplicate (n = 3) for each electrochemical determination. All of the potentials are reported with respect to the Ag/AgCl/Nafion electrode at an ambient temperature of 25 ± 2 °C, unless otherwise stated.

CNTf Synthesis and Fabrication of μ-ES. Vertically aligned forests of CNTs were grown by the CVD technique, and different widths of CNT forest were used to produce different diameter CNT fibers by the dry spinning process as reported earlier.[49,50] The produced CNT fiber has poor packing of CNTs as millions of nanotubes present within the fiber are held together by van der Waals attraction forces, and to increase the packing density and alignment among CNTs, the as-produced ∼40 and ∼94 μm diameter CNT fibers were soaked in acetone solvent for 96 h at 30 °C in an oven.[39] The microscopic images of HD-CNTf are shown in Figure 1A,B. The schematic of the μ-ES fabrication of three HD-CNTf rods has been summarized in Figure S1 (Supporting Information). The fabrication of μ-ES using HD-CNTf was carried out following the mechanical process reported in our earlier study.[39] Briefly, herein one 40 μm and two 94 μm diameter CNT fibers of 1.5 cm length were placed parallel to each other, with a distance of 2 mm, on tape. Then, the HD-CNTf attached tape was dipped vertically in Embed-812 monomer mixtures in a capsule-shaped 2 mL plastic vial and cured at 80−90 °C in an oven for 24 h. The cured fiber-embedded polymer capsule was microtomed orthogonally to the embedded CNT fiber into 40 μm thick slices with exposed open ends at both sides of the film. The HD-CNTf rods at the reverse side of the film were connected separately to conductive metal wires using silver paste and encapsulated with epoxy resin for electrical insulation, while the exposed open ends of three HD-CNTf rods on the front side of the film were used as the working electrode (∼40 μm diameter), reference, and counter electrode (∼94 μm diameter) for the electrochemical determination of the analyte. Bare HD-CNTf rod cross sections were used as working and counter electrodes, while the Ag/AgCl/Nafion-coated HD-CNTf rod cross section was used as the quasi-reference electrode. The micrographs of polymer-embedded three HD-CNTf rod μ-ES, in red circles, are shown in Figure 1C. Figure 1D displays the higher magnification image of HD-CNTf rod working electrode surface, confirming the high-density packing of CNTs within the fiber. The optical image of μ-ES and size comparison with scale parameters is shown in Figure 1E.

Fabrication of the HD-CNTf Rod Quasi-Reference Electrode. The exposed open ends of one ∼94 μm HD-CNTf rod was first electrochemically coated with Ag nanoparticles (NPs) using optimized 30 mM $AgNO_3$ in 1 M NH_3 solution with the help of a platinum wire and porous-junction Ag/AgCl as counter and reference electrode, respectively. The coatings of AgNPs were carried out by applying an optimized reduction potential at −300 mV for 30 s and then rinsed with DI water and dried under ambient room temperature. The FE-SEM images of AgNPs-electroplated HD-CNTf rod are shown in Figure 2A,B. Higher magnification images reveal the micron size of AgNPs coated on the HD-CNTf rod. Then, AgNPs-coated cross section of the HD-CNTf rod was treated with 50 mM $FeCl_3$ for 90 s to form a thin layer of AgCl on the surface and further rinsed with DI water and dried at room temperature (Figure 2C). The formation of the layer of AgCl was also confirmed by energy-dispersive X-ray analysis (EDAX), as shown in the Supporting Information, Figure S2A.

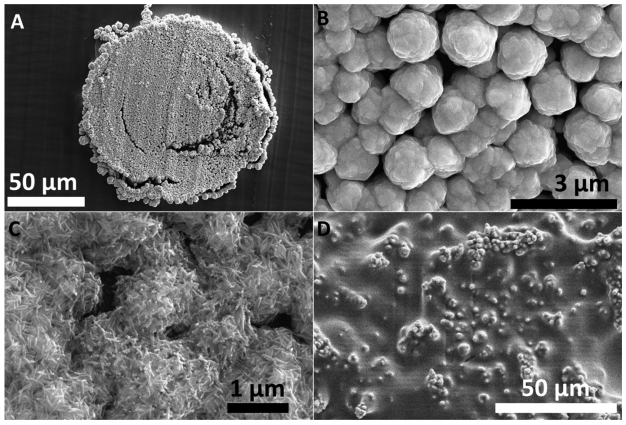

Figure 2. FE-SEM images of (A) AgNPs-coated ∼94 μm HD-CNTf rod embedded in an inert polymer, (B) high magnification of image A, (C) after the formation of the Ag/AgCl layer by drop casting $FeCl_3$ and (D) after the Nafion coating on the Ag/AgCl-plated HD-CNTf reference electrode.

https://doi.org/10.1021/acs.analchem.1c00360
Anal. Chem. 2021, 93, 7439−7448

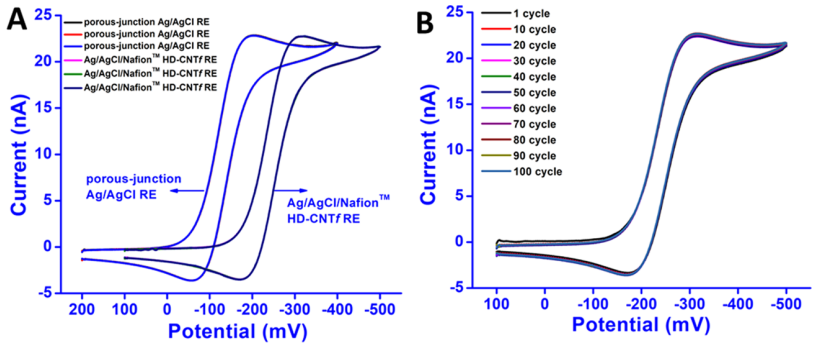

Figure 3. Cyclic voltammograms of 5 mM $[Ru(NH_3)_6]^{3+}$ in 50 mM KCl (A) for a comparative evaluation of the Ag/AgCl/Nafion-coated HD-CNTf rod quasi-reference electrode on the right and the commercial porous-junction Ag/AgCl reference electrode on the left with HD-CNTf rod cross sections as the working and counter electrodes and (B) at HD-CNTf rod μ-ES recorded for 1−100 cycles at 100 mV s^{-1}.

To protect their integrity and avoid degradation of the Ag/AgCl layer formed on the reference electrode during electrochemical calibration studies, 0.5 μL of 5% Nafion solution was drop casted onto the Ag/AgCl-coated HD-CNTf rod surface (Figure 2D). The Nafion-coated surface was dried at room temperature for 12 h and then cured in an oven at 90 °C for 1 h. The Nafion coating helps to maintain the integrity of the Ag/AgCl surface and provide the stable potential for extensive electrochemical testing for several days.[73] The EDAX data of the Ag/AgCl/Nafion quasi-reference electrode is shown in the Supporting Information, Figure S2B. During the electroplating of Ag nanoparticles, it is important to note that the CNT cross section should be fully covered with Ag nanoparticles to get stable and reproducible results. An incomplete or partial coating of the Ag/AgCl film over the CNT cross section gave irreproducible voltammograms, where shifting in peak potential was observed frequently. Therefore, the optimization of $AgNO_3$ concentration and deposition time is important to prepare a thick and fully covered Ag/AgCl film over the CNT cross section to get potential stability in test conditions.

RESULTS AND DISCUSSION

An important factor for CNT-based sensor fabrication is its purity and metal−catalyst free nature that have been reported in our recent study[39] confirming the absence of detectable metal catalyst and showed a significant increment in the D/G ratio at the cross section compared to the sidewall of HD-CNTf. The EDAX characterization of the HD-CNTf cross section showed 17 atomic % of oxygen groups confirming the presence of oxygen functionalities bound to the open-ended or defective sites (sp^3 carbon) of the CNTs after reaction with atmospheric O_2 or H_2O. The EDAX details are shown in the Supporting Information, Figure S3.

Ag/AgCl/Nafion-Coated HD-CNTf Rod Electrode. The reference electrode based on Ag/AgCl is widely used for electroanalytical studies due to its easy fabrication and minimal toxicity. The conventional porous-junction Ag/AgCl reference electrode shows excellent stability and reliability, but has drawbacks, i.e., leakage of liquid electrolyte, damage of porous junction (frit), and mechanically fragile glass body. The use of the solid-state quasi-reference electrode based on Ag/AgCl is free from internal filling solution, therefore offers an advantage over the conventional porous-junction Ag/AgCl reference electrode. The commercially available Ag/AgCl-based solid-state quasi-reference electrodes provide excellent resistance to most commonly used organic solvents, heat resistant up to 140 °C, 16 bar overpressure, and can be stored dry.[74−76] Its fabrication can be miniaturized and has been reported with in vivo studies,[77] disposable sensors, biosensor,[78,79] pH sensors,[74,78] and glucose biosensors for self-testing.[80,81] In this study, CNT rod-based reference electrode allows the microfabrication of the μ-ES sensor and does not require an internal filling solution.

The Ag/AgCl/Nafion-coated HD-CNTf rod electrode was evaluated as a quasi-reference electrode compared to the standard porous-junction Ag/AgCl commercial reference electrode by recording CVs in redox analyte, i.e., 5 mM $[Ru(NH_3)_6]^{3+}$ and 50 mM KCl (1:1 ratio) at a scan rate of 100 mV s^{-1}. The HD-CNTf rods embedded in the polymer matrix were used as the working (~40 μm diameter) and counter electrodes (~94 μm diameter). The redox potential of the voltammogram recorded at the HD-CNTf rod μ-ES shifted negatively by around ~110 mV in comparison to the commercial porous-junction Ag/AgCl reference electrode, as shown in Figure 3A. The difference in redox peak potential can be attributed to the internal filling solution of the commercial porous-junction reference electrode (3 M NaCl). The recorded three repetitive CVs showed overlap voltammograms for respective reference electrodes without any fluctuation in peak potential and peak current, as shown in Figure 3A.

The commercial solid-state quasi-reference electrode based on Ag/AgCl was also tested by recording the CVs in 1:1 ratio of 5 mM $[Ru(NH_3)_6]^{3+}$ and 50 mM KCl using the HD-CNTf rod working and counter electrodes in μ-ES. The observed voltammograms were similar in terms of potential and peak height to the CVs observed for the Ag/AgCl/Nafion-coated HD-CNTf rod reference electrode. We attribute this similarity to the absence of internal filling solution in both cases. The optical images of the commercial porous-junction Ag/AgCl (3 M NaCl), solid-state Ag/AgCl, and μ-ES used in the current study are presented in Figure S4 (Supporting Information).

HD-CNTf Rod Working Electrode. To evaluate the electrochemical properties of the HD-CNTf rod working electrode, CVs were recorded in a 1:1 ratio solution of 5 mM $Ru(NH_3)_6Cl_3$ and 50 mM KCl at various scan rates ranging from 5 to 500 mV s^{-1}. Figure S5 (Supporting Information) shows the CVs at the HD-CNTf rod μ-ES for the reduction of $[Ru(NH_3)_6^{3+/2+}]$ for the scan rates of 5−500 mV s^{-1}. For the scan rate range of 5−20 mV s^{-1}, the forward and reverse scans were essentially sigmoidal-shaped curves, which are characteristic of hemispherical diffusion (Figure S5A). Further incre-

https://doi.org/10.1021/acs.analchem.1c00360
Anal. Chem. 2021, 93, 7439−7448

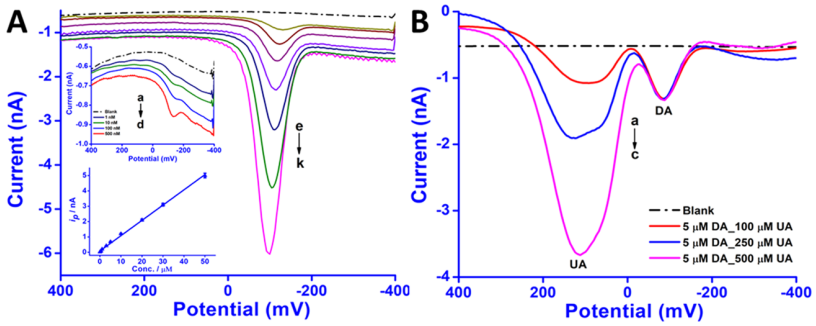

Figure 4. (A) SWVs recorded for increasing concentration of DA at (a) 0.001 μM, (b) 0.01 μM, (c) 0.1 μM, (d) 0.5 μM, (e) 1 μM, (f) 3 μM, (g) 5 μM, (h) 10 μM, (i) 20 μM, (j) 30 μM, and (k) 50 μM in pH 7.2 phosphate buffer using HD-CNTf rod μ-ES. The upper inset graph is the SWVs of lower concentration dopamine, and the lower inset graph is the observed calibration plot between [concentration] and i_p. (B) SWVs showing interference of both AA (a) 50 μM, (b) 250 μM, and (c) 500 μM (peak not observed) and UA (a) 100 μM, (b) 250 μM, and (c) 500 μM at fixed 5 μM concentration of DA. Blank is shown by a dotted line.

ment in the scan rate from 20 to 500 mV s^{-1} reveals small gentle peaks rather than steady-state currents for both the forward and reverse scans. With increasing the scan rate, the mass transport is likely to have an increased contribution from planar diffusion.[39,82,83] Even so, the observed signals cannot be considered in any way transient; therefore, the half-peak potential is convenient to calculate the rate of electron transfer. The observed responses were following Nernstian behavior over the entire scan rate range from 5 to 500 mV s^{-1}, with the differences in the 1/4- and 3/4-wave potential, $E_{1/4} - E_{3/4}$, in the range 59−60 mV, confirming the reversible and fast electron kinetics for the redox electrochemical investigation. At a lower scan rate (inset Figure S5A), the HD-CNTf rod working electrode shows a truly sigmoidal steady state-state limiting current with a magnitude of several nanoamperes. The limiting current, I_{lim}, at the cross section of HD-CNTf rod is given by eq 1.

$$I_{lim} = 4nFDaC \quad (1)$$

where n refers to the number of electrons transferred per redox event, diffusion coefficient (D) of 8.2 × 10^{-6} cm^2 s^{-1},[84,85] F is the Faraday constant 96485 C mol^{-1}, C is the concentration 2.5 mM for $[Ru(NH_3)_6]Cl_3$, and radius (a) for the cross section of 20 μm. From eq 1, the calculated limiting current is ∼16 nA, which is the same magnitude observed in the voltammogram.

To test the stability of the complete μ-ES, HD-CNTf rod working electrode, Ag/AgCl/Nafion-coated HD-CNTf rod quasi-reference electrode, and HD-CNTf rod counter electrode, continuous CVs in 1:1 ratio solution of 5 mM $Ru(NH_3)_6Cl_3$ and 50 mM KCl were recorded for 100 cycles at 100 mV s^{-1} scan rate, as shown in Figure 3B. The observed data showed constant peak potential and current without any deviation as all recorded voltammograms overlapped each other confirming that, using the presented μ-ES, the Ag/AgCl/Nafion-coated HD-CNTf rod as the quasi-reference electrode and bare HD-CNTf rod cross section as the working and counter electrodes are stable and suitable for multiple electroanalytical applications.

Detection of Biomolecules and Heavy Metal. The presented HD-CNTf rod μ-ES consisting of bare ∼40 and ∼94 μm diameter HD-CNTf rods as the working and counter electrodes, respectively, and a 100 μm diameter HD-CNTf rod coated with Ag/AgCl/Nafion as the quasi-reference electrode was applied to the determination of dopamine, NADH, and furosemide in 0.1 M phosphate buffer and lead ion (Pb^{2+}) in tap water.

Dopamine (DA). Cyclic voltammetry provides useful insights over electron transfer kinetics, qualitative analysis of redox processes, and reversibility of reactions. To understand the nature of the electrochemical reactions at the electrode surface, CVs were recorded for 20 μM DA in 0.1 M phosphate buffer solution of pH 7.2 at various scan rate ranges from 5 to 200 mV s^{-1}, as shown in Figure S6 (Supporting Information). The observed CVs at the μ-ES show well-defined oxidation and reduction peaks for DA at −65 and −94 mV vs Ag/AgCl/Nafion-coated HD-CNTf rod, respectively. The peak-to-peak separation values (ΔE_p) near to ∼30 mV confirm the two-electron oxidation process of DA with fast electron transfer kinetics at the HD-CNTf rod μ-ES. The anodic peak current of DA was found to increase linearly with increasing scan rates (inset of Figure S6, Supporting Information). The plots of peak current (i_p) vs scan rate (ν) and log i_p vs log ν were found to be a straight line and are represented by the following eqs 2 and 3

$$i_p\ (\text{nA}) = (0.0116 \pm 0.0003)(\nu\ (\text{mV s}^{-1})) - (0.0109 \pm 0.0115) \quad R^2 = 0.994 \quad (2)$$

$$i_p\ (\text{nA}) = (0.8702 \pm 0.048)(\log \nu\ (\text{mV s}^{-1})) - (1.6888 \pm 0.090) \quad R^2 = 0.982 \quad (3)$$

The linearity of i_p vs ν (shown in the inset of Figure S5) and the slop value of ∼0.870 (> 0.5) for log i_p vs log ν confirm that the oxidation of DA proceeds via an adsorption-controlled process at the HD-CNTf rod μ-ES. The open-end CNT sites at the HD-CNTf rod μ-ES have more oxygen-containing functional groups, which work as active adsorption sites and lead the adsorption-controlled redox process of dopamine.[47,57]

The calibration study of DA was performed using square wave voltammetry at the HD-CNTf rod μ-ES in 0.1 M phosphate buffer of pH 7.2. The observed SWVs show that the dopamine oxidation peak current increases linearly with the concentration over the entire range from 1 nM to 50 μM, as shown in Figure 4A, and can be expressed by the following linear eq 4

$$i_p\ (\text{nA}) = 0.0995[C_{\text{dopamine}}(0.001 - 50\ \mu\text{M})] + 0.0854 \quad (R^2 = 0.998) \quad (4)$$

https://doi.org/10.1021/acs.analchem.1c00360
Anal. Chem. 2021, 93, 7439−7448

where i_p is the peak current (nA) and C is the concentration of DA (μM). The limit of detection (LOD) was calculated using $3\sigma/b$, where σ is the standard deviation of the blank solution and b is the slope of the calibration plot and was found to be 0.5 nM. The proposed μ-ES allows highly sensitive and lower potential detection of DA, which can be attributed to the oxygen functional groups at the open-end sites of the HD-CNTf rod. The complete calibration study of DA was performed on a single HD-CNTf rod μ-ES, and the measurements were made three times for all individual concentrations showing the stability and robustness of the proposed sensor for multiple analysis.

Selective detection of analytes is an important factor for the practical applicability of the sensor in biological and chemical research. The HD-CNTf rod μ-ES was tested for selective determination of DA in the presence of potential interference analytes, i.e., ascorbic acid (AA) and uric acid (UA) in Figure 4B. Both AA and UA are common metabolite molecules present in human biological fluids, i.e., blood and urine at higher concentrations than DA and oxidize at similar potentials to DA which can alter the voltammetric response of the sensor and affect the true quantitative estimation of DA. The SWVs in a mixture of 5 μM DA were recorded with increasing concentrations of AA and UA up to 500 μM, as shown in Figure 4B. The observed results clearly demonstrate the selective detection of DA, where the electrochemical oxidation of DA was not affected in the presence of 100 times higher concentrations of AA and UA. In the observed voltammograms, DA and UA showed significant peaks while AA oxidation was completely diminished at the HD-CNTf cross section surface, which can be explained by the electrostatic barrier at the CNT cross-sectional surface. The negatively charged oxygen and carboxylic functional groups present at the open ends or defective sites of CNTs repel negatively charged anionic AA.[60] The electrostatic repulsion of anionic AA inhibits the adsorption and charge transfer process to the CNT cross-sectional surface, and thereby AA oxidation peak was effectively suppressed. The observed data reveals the safe application of the proposed μ-ES for the sensitive detection of DA in pharmaceutical preparations and biological fluids.

β-Nicotinamide Adenine Dinucleotide (NADH). Over 300 dehydrogenases are known which are dependent on the coenzyme, NADH, and its oxidized form NAD^+. The electrochemical oxidation of NADH is of great interest due to its significance in a wide diversity of dehydrogenase-based biosensors. Direct oxidation of NADH at unmodified conventional carbon-based surfaces takes place at high overpotentials (>+500 mV) owing to the slow electron transfer kinetics.[32,86−89] The oxidation of NADH at high overpotentials also leads to fouling of electrode surface associated with the accumulation of the reaction product, which affects the NADH current response stability.[32,87,89] To overcome this problem, initially much effort had been devoted toward modifying the electrode surface with redox mediators, which reduces the overpotential of NADH oxidation and prevents the possibility of electrode surface fouling.[87,90] However, the use of mediators exhibited intrinsic problems related to limited stability and their leaching from the electrodes. Later approaches of using different forms of carbon, i.e., CNTs and pyrolytic graphite, greatly reduce the overpotential of NADH oxidation, which was ascribed to the electrocatalytic effects of edge sites of CNTs and pyrolytic graphite electrodes.[32,86,91] In this work, the μ-ES sensor exposed highly densified open ends of CNTs at the electrode−electrolyte interface, which may lead to more facile electron transfer, were investigated for NADH oxidation.

To understand the nature of NADH oxidation on the electrode surface, a cyclic voltammogram of 5 mM NADH was recorded in 0.1 M phosphate buffer of pH 7.2 at 100 mV s^{-1} scan rate, as shown in Figure 5A. The oxidation of NADH at

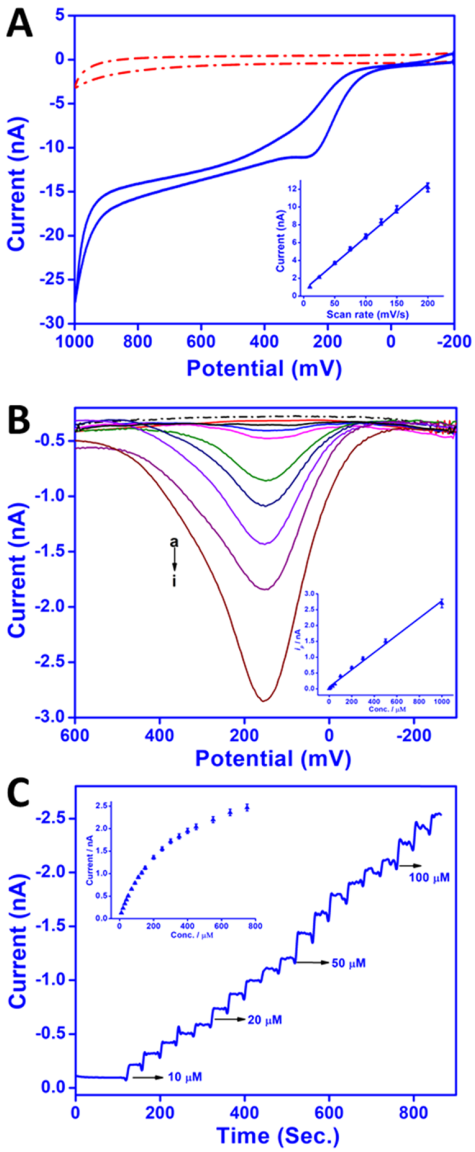

Figure 5. (A) CV recorded for 5 mM NADH at 100 mV s^{-1} (solid line); (B) SWVs for different concentrations of NADH: (a) 1 μM, (b) 10 μM, (c) 30 μM, (d) 50 μM, (e) 100 μM, (f) 200 μM, (g) 300 μM, (h) 500 μM, and (i) 1000 μM; and (C) amperometric response observed for different concentrations of NADH. All data was recorded in 0.1 M phosphate buffer of pH 7.2 at the HD-CNTf rod μ-ES. Observed calibration plots are between [C] and i_p (inset). Blanks are shown by a dotted line.

the HD-CNTf rod occurs at ~250 mV vs Ag/AgCl/Nafion-coated HD-CNTf rod, and in reverse scan, no peak for NADH is observed showing the irreversible oxidation behavior of NADH. The potential of the standard porous-junction Ag/AgCl reference electrode is 110 mV more positive relative to the Ag/AgCl/Nafion-coated HD-CNTf rod (Figure 3A), and if

https://doi.org/10.1021/acs.analchem.1c00360
Anal. Chem. 2021, 93, 7439−7448

we correct our observed peak potential (250 mV vs Ag/AgCl/Nafion-coated HD-CNTf rod, 100 mV s^{-1}) for NADH oxidation corresponding to the standard Ag/AgCl reference electrode, the oxidation of NADH in this study occurs at ~360 mV. The observed peak potential is in excellent agreement range with that observed by researchers at the CNT-modified glassy carbon electrode (GCE),[86,91] boron-doped CNTs,[88] edge plane, and CNT-modified basal plane pyrolytic graphite electrodes.[32] The high proportion of edge site defects or open ends of CNTs with oxygen-rich functional groups showed high electrocatalytic activity toward the oxidation of NADH and therefore were attributed responsibility for the significant reduction in the oxidation potential of NADH.[32,86,91]

Further, the effect of the scan rate on oxidation peak current of NADH was examined in the range 10−200 mV s^{-1} using HD-CNTf rod μ-ES. The oxidation peak current was found to increase linearly with the increasing scan rate (inset Figure 5A) and the dependence of peak current (i_p) on the scan rate (ν) can be expressed by the following eq 5

$$i_p\ (\mathrm{nA}) = (0.0594 \pm 0.0013)(\nu\ (\mathrm{mV\,s^{-1}})) + (0.6768 \pm 0.1466) \quad R^2 = 0.997 \tag{5}$$

The linear relation between i_p versus ν indicates that electrode reaction is adsorption controlled. To further confirm the adsorption-controlled nature of electrode reaction, a graph was plotted between log i_p vs log ν, which can be expressed by eq 6

$$i_p\ (\mathrm{nA}) = (0.8407 \pm 0.0067)(\log \nu\ (\mathrm{mV\,s^{-1}})) - (0.8492 \pm 0.012) \quad R^2 = 0.999 \tag{6}$$

The plot was linear and the observed slop value ~0.840 (>0.5) confirms that the oxidation of NADH at HD-CNTf rod μ-ES follows an adsorption-controlled pathway.

SWV was used to investigate the μ-ES properties during NADH oxidation under optimum conditions. Figure 5B displays SWVs of NADH with different concentrations, and the oxidation peak current was found to increase as the concentration of NADH was increased and a linear relationship with NADH concentration was observed in a wide range of 1−1000 μM (Figure 5B inset). The linear relationship of NADH concentration versus peak current can be expressed by the following eq 7

$$i_p\ (\mathrm{nA}) = 0.0027[C_{\mathrm{NADH}}(1 - 1000\ \mu\mathrm{M}] + 0.06 \quad R^2 = 0.994 \tag{7}$$

where i_p is the peak current (nA) and C is the concentration of NADH (μM). The LOD was calculated using $3\sigma/b$ and found to be 18 nM. The observed wide linear range can be useful in developing further applications based on dehydrogenase.

The reported μ-ES offers lower oxidation potential; therefore, further low-potential amperometric measurement of NADH at HD-CNTf rod was also explored. Figure 5C displays the current−time response from additions of NADH to a 0.1 M phosphate buffer of pH 7.2 solution under conditions where the potential was kept at +300 mV vs Ag/AgCl/Nafion-coated HD-CNTf rod. Figure 5C presents the amperometric response of the HD-CNTf rod at +300 mV to the successive addition of NADH into a stirred buffer solution. It was observed that the HD-CNTf rod responds very rapidly, immediately after the addition of NADH, and the anodic current increased and produced a steady state within 5−6 s. From the observed data, the HD-CNTf rod μ-ES was found to exhibit a linear range up to 250 μM concentration of NADH with a correlation coefficient of 0.980 and a slope of 6 pA μM^{-1}. The faster amperometric response time can be attributed to the open-end sites of the HD-CNTf rod, which facilitate the faster charge transport. The amperometric response of the proposed μ-ES leveled off at a high concentration of NADH, which can be implied to the reduction of active surface area of the electrode by the adsorption of oxidation product NAD^+ with time.[88,91,92] In the case of SWVs, the observed calibration graph is linear (inset Figure 5B) which might be due to cleaning of the working electrode using CPE at 500 mV for 60 s after recording each SWV, which gives a fresh CNT surface to record the new SWV for NADH calibration study. The high abundance of oxygen-containing functional groups at the cross section of the HD-CNTf rod provides electroactive sites with negative charges, which are good for adsorption of NAD^+. The amperometric response of NADH oxidation at the cross section of HD-CNTf rod is similar to the reported behavior of CNTs-based electrodes.[88,91,92]

Furosemide. Furosemide, a diuretic drug, that increases the urine flow and sodium excretion used in the treatment of several diseases and syndromes. Like other diuretic drugs, furosemide is abused by athletes for rapid weight loss and is also used to mask the presence of other doping agents by reducing their concentration in the urine. Therefore diuretics are included in the list of prohibited substances by the World Anti-Doping Agency (WADA).[93] Furosemide is the most common drug detected in athlete samples and its occurrence has increased over the years.[93] Only a few studies on the electrochemical determination of furosemide have been reported, where most of them are lacking a quantification range[67,94−96] and are using complex electrode modifications.[97,98] This motivated us to study this diuretic drug on the proposed μ-ES. The sensitive detection of furosemide was performed using the SWV technique in 0.1 M phosphate buffer of pH 2.2. The effect of supporting electrolyte was examined over the pH range of 2.2−7.2 and observed data showed two well-defined peaks that shifted toward less positive potentials together with a decrease in peak current with increasing pH of the supporting electrolyte. The largest and well-defined peaks were observed at pH 2.2. Therefore, a phosphate buffer of pH 2.2 was selected as the supporting electrolyte for the quantification.

The SWVs recorded with increasing concentration of furosemide in 0.1 M phosphate buffer of pH 2.2 at HD-CNTf rod μ-ES showed the linear increment in both oxidation currents, i.e., peak (i) at ~720 mV and peak (ii) at ~940 mV, as shown in Figure 6. Based on the voltammetry results reported earlier, furosemide is electro-oxidized via two, one-electron steps and, therefore, two rate-limiting steps are involved in the electrochemical oxidation of furosemide. There were observed two oxidation peaks at the HD-CNTf rod μ-ES for furosemide, each associated with the transfer of one electron.[67,68,99] The second peak (ii) is relatively more intense and showed a larger increment with an increase in concentration than peak (i). Therefore, the peak currents of peak (ii) were used for quantification. The proposed HD-CNTf rod μ-ES shows two clear oxidation peaks for 100 nM concentration of furosemide, which is well below the minimum required performance level (MRPL; ~200 ng mL^{-1} or 600 nM) of diuretics set by WADA.[100] Concentration inves-

https://doi.org/10.1021/acs.analchem.1c00360
Anal. Chem. 2021, 93, 7439−7448

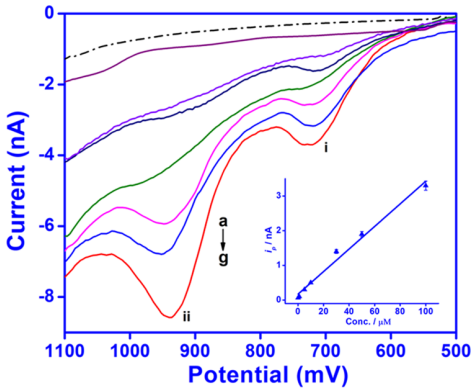

Figure 6. SWVs for various concentrations of furosemide: (a) 0.1 μM, (b) 1 μM, (c) 5 μM, (d) 10 μM, (e) 30 μM, (f) 50 μM, and (g) 100 μM on the HD-CNTf rod in 0.1 M phosphate buffer of pH 2.2. Observed calibration plots are between [C] and i_p (inset). Blank is shown by the dotted line.

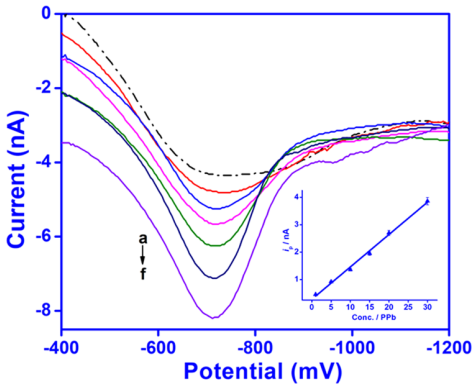

Figure 7. SWASVs for Pb^{2+} in tap water at the HD-CNTf rod μ-ES: (a) 1 ppb, (b) 5 ppb, (c) 10 ppb, (d) 15 ppb, (e) 20 ppb, and (f) 30 ppb of Pb^{2+}. Accumulation time: 120 s; deposition potential: −1.2 V. Observed calibration plots are between [C] and i_p (inset). Blank is shown by the dotted line.

tigations were carried out in the range of 100 nM to 100 μM, and the peak current (peak ii) dependence on concentration can be expressed as eq 8

$$i_p\ (\text{nA}) = 0.032[C_{\text{furosemide}}(0.1 - 100\ \mu\text{M}] + 0.1681$$
$$R^2 = 0.986 \quad (8)$$

where i_p is the peak current (nA) and C is the concentration of furosemide (μM). The LOD using $3\sigma/b$ was observed to be 2 nM. The observed results indicate the strong electrocatalytic effect of the HD-CNT rod cross section toward the furosemide electro-oxidation. Thus, with the wide linear range and detection of lower concentrations than the MRPL limit set by WADA,[100] the proposed HD-CNTf rod μ-ES can be used for the determination of furosemide in human biological fluids and pharmaceutical formulations.

The stability and reproducibility study results of the proposed HD-CNTf rod μ-ES for the biomolecules and heavy metal are given in Section 7 of the Supporting Information. The observed results indicated the good accuracy and reproducibility of the proposed HD-CNTf rod μ-ES.

Heavy Metal Detection. Lead contamination in drinking water is a major global issue. In the United States, lead service pipelines and lead-containing plumbing materials are the largest contributors of lead contamination in the residential drinking water supply. The sensitive detection of Pb^{2+} was performed using SWASV in tap water without adding any supporting electrolyte and reagent. The tap water sample was collected from a faucet in Crosley Tower, University of Cincinnati having pH value and conductivity of 8.3 and 285 μS cm^{-1}, respectively. The applied deposition potential −1200 mV is sufficiently negative to reduce Pb^{2+} along with other heavy metal ions if present in tap water, and the optimized 120 s deposition time was selected to balance calibration range along with the lower detection limit. The well-defined stripping peaks were obtained in tap water at HD-CNTf rod μ-ES for spiked lead ions over the concentration range of 1−30 ppb, as shown in Figure 7. The stripping peak current was found to increase linearly versus metal ion concentration, and the correlation equation can be expressed as eq 9

$$i_p\ (\text{nA}) = 0.118[C_{Pb^{2+}}(1 - 30\ \text{ppb})] + 0.2808$$
$$R^2 = 0.996 \quad (9)$$

where i_p is the stripping peak current (nA) and C is the concentration of Pb^{2+} metal ions in ppb (parts per billion) in tap water. The LOD was calculated to be 400 ppt for Pb^{2+}in tap water. The proposed HD-CNTf rod μ-ES successfully quantified 1 ppb concentration of lead ions in tap water without adding any supporting electrolyte, which is well below the allowable limits of the World Health Organization (WHO; 10 ppb) and United States-Environment Protection Agency (US-EPA; 15 ppb), showing the high sensitivity and robustness of the μ-ES for onsite application of heavy metal detection. In our most recent study, we reported a microsensor that consisted of six CNT fiber cross sections, where each cross section had a diameter of 70 μm and was employed along with the commercial Ag/AgCl reference electrode and platinum wire as the counter electrode, to detect Pb^{2+}. This working electrode had a linear range response of 0.1−50 ppb.[101] On the other hand, in the current study, the working electrode is made up of a single 40 μm fiber cross section, thus limiting the linear range of Pb^{2+} detection in tap water to 1−30 ppb. Accommodating multiple microelectrodes as working electrodes within the μ-ES resulted is challenging; as a result, a single working electrode is employed, but still the reported μ-ES showed excellent sensitivity.

CONCLUSIONS

The first μ-ES where all three microelectrodes were made of highly densified carbon nanotubes fiber (HD-CNTf) cross sections called rods (~40 μm length) with exposed open ends at electrolyte interface has been developed. The cross section of HD-CNTf rods have microsized diameter, where the working electrode (~40 μm diameter) and counter electrode (~94 μm diameter) were used as a bare open-end CNT surface, while the quasi-reference electrode (~94 μm diameter) cross section was electroplated with Ag/AgCl nanoparticles followed by the Nafion coating. The CV measurements in the redox analyte showed the fast electron transfer kinetics at the HD-CNTf rod cross section working electrode, and it was found that the Nafion/Ag/AgCl-coated quasi-reference electrode showed sufficiently stable potential.

https://doi.org/10.1021/acs.analchem.1c00360
Anal. Chem. 2021, 93, 7439−7448

The proposed μ-ES was evaluated for the electrochemical determination of biologically important biomolecules, a diuretic drug, and an environmentally toxic heavy metal. The electrochemical determination of DA, NADH, furosemide in phosphate buffer and lead ion detection in tap water was performed using different voltammetric techniques, i.e., CV, SWV, amperometry, and SWASV. From the results, it can be concluded that the developed HD-CNTf rod μ-ES offers a wide linear range, excellent sensitivity, and very low limits of detection for the electrochemical sensing of DA, NADH, furosemide, and lead ions. The low quantification range of biomolecules and the 1 ppb quantification of Pb^{2+} in tap water without adding any supporting electrolyte show the promising applicability and robustness of the proposed μ-ES for on-site applications. The validation characteristics of the presented microsensor are shown in Table S1 (Supporting Information). This novel μ-ES configuration can be extremely useful for the generic electrochemical and biosensing of various biologically important analytes with potentially single drop sample volume and therefore can be used in widespread clinical applications for delivering the diagnostic information in rapid, simple, and low cost, early point-of-care screenings.

■ ASSOCIATED CONTENT

Supporting Information

The Supporting Information is available free of charge at https://pubs.acs.org/doi/10.1021/acs.analchem.1c00360.

Schematic of HD-CNTf rod μ-ES fabrication; EDAX data of the quasi-reference electrode and HD-CNTf cross section; CV characterization; and stability and reproducibility (PDF)

■ AUTHOR INFORMATION

Corresponding Author

Noe T. Alvarez − *Department of Chemistry, University of Cincinnati, Cincinnati, Ohio 45221, United States;* orcid.org/0000-0002-8392-1483; Phone: 513-556-9370; Email: alvarene@ucmail.uc.edu

Authors

Pankaj Gupta − *Department of Chemistry, University of Cincinnati, Cincinnati, Ohio 45221, United States;* orcid.org/0000-0001-7689-4352

Connor E. Rahm − *Department of Chemistry, University of Cincinnati, Cincinnati, Ohio 45221, United States*

Benjamin Griesmer − *Department of Chemistry, University of Cincinnati, Cincinnati, Ohio 45221, United States*

Complete contact information is available at: https://pubs.acs.org/10.1021/acs.analchem.1c00360

Notes

The authors declare no competing financial interest.

■ ACKNOWLEDGMENTS

The authors are indebted to professorship start-up funds from the Department of Chemistry at the University of Cincinnati and NSF 2016484 grant under the NSF PFI-RP program. Special thanks to Prof. Vesselin Shanov and Prof. Elke Buschbeck for providing CNT fibers and microtome facilities, respectively.

■ REFERENCES

(1) Iijima, S. *Nature* **1991**, *354*, 56−58.
(2) Iijima, S.; Ichihashi, T. *Nature* **1993**, *363*, 603−605.
(3) Ajayan, P. M. *Chem. Rev.* **1999**, *99*, 1787−1800.
(4) Rao, C. N. R.; Satishkumar, B. C.; Govindaraj, A.; Nath, M. *ChemPhysChem* **2001**, *2*, 78−105.
(5) Peigney, A.; Laurent, C.; Flahaut, E.; Bacsa, R. R.; Rousset, A. *Carbon* **2001**, *39*, 507−514.
(6) Gooding, J. J. *Electrochim. Acta* **2005**, *50*, 3049−3060.
(7) Swamy, B. E. K.; Venton, B. J. *Analyst* **2007**, *132*, 876.
(8) Dumitrescu, I.; Unwin, P. R.; Macpherson, J. V. *Chem. Commun.* **2009**, *7345*, 6886.
(9) Schroeder, V.; Savagatrup, S.; He, M.; Lin, S.; Swager, T. M. *Chem. Rev.* **2019**, *119*, 599−663.
(10) Zhao, Q.; Gan, Z.; Zhuang, Q. *Electroanalysis* **2002**, *14*, 1609−1613.
(11) Britto, P. J.; Santhanam, K. S. V.; Ajayan, P. M. *Bioelectrochem. Bioenerg.* **1996**, *41*, 121−125.
(12) Wang, J. *Electroanalysis* **2005**, *17*, 7−14.
(13) Cao, Q.; Puthongkham, P.; Venton, B. J. *Anal. Methods* **2019**, *11*, 247−261.
(14) Beitollahi, H.; Movahedifar, F.; Tajik, S.; Jahani, S. *Electroanalysis* **2019**, *31*, 1195−1203.
(15) Merkoçi, A.; Pumera, M.; Llopis, X.; Pérez, B.; del Valle, M.; Alegret, S. *TrAC, Trends Anal. Chem.* **2005**, *24*, 826−838.
(16) Wang, J.; Musameh, M.; Lin, Y. *J. Am. Chem. Soc.* **2003**, *125*, 2408−2409.
(17) Wu, K.; Hu, S.; Fei, J.; Bai, W. *Anal. Chim. Acta* **2003**, *489*, 215−221.
(18) Zhang, M.; Smith, A.; Gorski, W. *Anal. Chem.* **2004**, *76*, 5045−5050.
(19) Valentini, F.; Amine, A.; Orlanducci, S.; Terranova, M. L.; Palleschi, G. *Anal. Chem.* **2003**, *75*, 5413−5421.
(20) Rubianes, M. D.; Rivas, G. A. *Electrochem. Commun.* **2003**, *5*, 689−694.
(21) Rivas, G. A.; Rubianes, M. D.; Pedano, M. L.; Ferreyra, N. F.; Luque, G. L.; Rodríguez, M. C.; Miscoria, S. A. *Electroanalysis* **2007**, *19*, 823−831.
(22) Sanghavi, B. J.; Srivastava, A. K. *Electrochim. Acta* **2010**, *55*, 8638−8648.
(23) Wang, J.; Musameh, M. *Analyst* **2004**, *129*, 1.
(24) Sánchez, S.; Pumera, M.; Cabruja, E.; Fàbregas, E. *Analyst* **2007**, *132*, 142−147.
(25) Rahm, C. E.; Torres-Canas, F.; Gupta, P.; Poulin, P.; Alvarez, N. T. *Electroanalysis* **2020**, *32*, 1533−1545.
(26) Barisci, J. N.; Wallace, G. G.; Baughman, R. H. *J. Electrochem. Soc.* **2000**, *147*, 4580.
(27) Bahr, J. L.; Yang, J.; Kosynkin, D. V.; Bronikowski, M. J.; Smalley, R. E.; Tour, J. M. *J. Am. Chem. Soc.* **2001**, *123*, 6536−6542.
(28) Li, J.; Cassell, A.; Delzeit, L.; Han, J.; Meyyappan, M. *J. Phys. Chem. B* **2002**, *106*, 9299−9305.
(29) Musameh, M.; Wang, J. *Anal. Chem.* **2003**, *75*, 2075−2079.
(30) Wohlstadter, J. N.; Wilbur, J. L.; Sigal, G. B.; Biebuyck, H. A.; Billadeau, M. A.; Dong, L.; Fischer, A. B.; Gudibande, S. R.; Jameison, S. H.; Kenten, J. H.; Leginus, J.; Leland, J. K.; Massey, R. J.; Wohlstadter, S. J. *Adv. Mater.* **2003**, *15*, 1184−1187.
(31) Moore, R. R.; Banks, C. E.; Compton, R. G. *Anal. Chem.* **2004**, *76*, 2677−2682.
(32) Banks, C. E.; Compton, R. G. *Analyst* **2005**, *130*, 1232−1239.
(33) Liu, Z.; Shen, Z.; Zhu, T.; Hou, S.; Ying, L.; Shi, Z.; Gu, Z. *Langmuir* **2000**, *16*, 3569−3573.
(34) Nugent, J. M.; Santhanam, K. S. V.; Rubio, A.; Ajayan, P. M. *Nano Lett.* **2001**, *1*, 87−91.
(35) Gooding, J. J.; Wibowo, R.; Liu; Yang, W.; Losic, D.; Orbons, S.; Mearns, F. J.; Shapter, J. G.; Hibbert, D. B. *J. Am. Chem. Soc.* **2003**, *125*, 9006−9007.
(36) Dai, L.; Patil, A.; Gong, X.; Guo, Z.; Liu, L.; Liu, Y.; Zhu, D. *ChemPhysChem* **2003**, *4*, 1150−1169.
(37) Lin, Y.; Lu, F.; Tu, Y.; Ren, Z. *Nano Lett.* **2004**, *4*, 191−195.

(38) Patolsky, F.; Weizmann, Y.; Willner, I. *Angew. Chem., Int. Ed.* **2004**, *43*, 2113−2117.
(39) Gupta, P.; Lazenby, R. A.; Rahm, C. E.; Heineman, W. R.; Buschbeck, E.; White, R. J.; Alvarez, N. T. *ACS Appl. Energy Mater.* **2019**, *2*, 8757−8766.
(40) Gupta, P.; Tsai, K.; Ruhunage, C. K.; Gupta, V. K.; Rahm, C. E.; JIANG, D.; Alvarez, N. T. *Anal. Chem.* **2020**, 8536−8545.
(41) Wang, J.; Deo, R. P.; Poulin, P.; Mangey, M. *J. Am. Chem. Soc.* **2003**, *125*, 14706−14707.
(42) Tu, Y.; Lin, Y.; Ren, Z. F. *Nano Lett.* **2003**, *3*, 107−109.
(43) Viry, L.; Derré, A.; Garrigue, P.; Sojic, N.; Poulin, P.; Kuhn, A. *Anal. Bioanal. Chem.* **2007**, *389*, 499−505.
(44) Wang, J.; Liu, G.; Jan, M. R. *J. Am. Chem. Soc.* **2004**, *126*, 3010−3011.
(45) Gong, K.; Chakrabarti, S.; Dai, L. *Angew. Chem., Int. Ed.* **2008**, *47*, 5446−5450.
(46) Harreither, W.; Trouillon, R.; Poulin, P.; Neri, W.; Ewing, A. G.; Safina, G. *Anal. Chem.* **2013**, *85*, 7447−7453.
(47) Yang, C.; Trikantzopoulos, E.; Jacobs, C. B.; Venton, B. J. *Anal. Chim. Acta* **2017**, *965*, 1−8.
(48) Jiang, K.; Li, Q.; Fan, S. *Nature* **2002**, *419*, 801.
(49) Alvarez, N. T.; Miller, P.; Haase, M.; Kienzle, N.; Zhang, L.; Schulz, M. J.; Shanov, V. *Carbon* **2015**, *86*, 350−357.
(50) Alvarez, N. T.; Miller, P.; Haase, M. R.; Lobo, R.; Malik, R.; Shanov, V. *Carbon* **2019**, *144*, 55−62.
(51) Zhu, Z.; Song, W.; Burugapalli, K.; Moussy, F.; Li, Y.-L.; Zhong, X.-H. *Nanotechnology* **2010**, *21*, No. 165501.
(52) Zhao, D.; Guo, X.; Wang, T.; Alvarez, N.; Shanov, V. N.; Heineman, W. R. *Electroanalysis* **2014**, *26*, 488−496.
(53) Zhao, D.; Siebold, D.; Alvarez, N. T.; Shanov, V. N.; Heineman, W. R. *Anal. Chem.* **2017**, *89*, 9654−9663.
(54) Wang, K.; Fishman, H. A.; Dai, H.; Harris, J. S. *Nano Lett.* **2006**, *6*, 2043−2048.
(55) Vitale, F.; Summerson, S. R.; Aazhang, B.; Kemere, C.; Pasquali, M. *ACS Nano* **2015**, *9*, 4465−4474.
(56) Schmidt, A. C.; Wang, X.; Zhu, Y.; Sombers, L. A. *ACS Nano* **2013**, *7*, 7864−7873.
(57) Jacobs, C. B.; Ivanov, I. N.; Nguyen, M. D.; Zestos, A. G.; Venton, B. J. *Anal. Chem.* **2014**, *86*, 5721−5727.
(58) Bucher, E. S.; Wightman, R. M. *Annu. Rev. Anal. Chem.* **2015**, *8*, 239−261.
(59) Roberts, J. G.; Moody, B. P.; McCarty, G. S.; Sombers, L. A. *Langmuir* **2010**, *26*, 9116−9122.
(60) Zestos, A. G. *Int. J. Electrochem.* **2018**, *2018*, 1−19.
(61) Weese, M. E.; Krevh, R. A.; Li, Y.; Alvarez, N. T.; Ross, A. E. *ACS Sens.* **2019**, *4*, 1001−1007.
(62) Chou, A.; Böcking, T.; Singh, N. K.; Gooding, J. J. *Chem. Commun.* **2005**, 842−844.
(63) Keerthi, M.; Boopathy, G.; Chen, S.-M.; Chen, T.-W.; Lou, B.-S. *Sci. Rep.* **2019**, *9*, No. 13075.
(64) Huang, Q.; Lin, X.; Tong, L.; Tong, Q. X. *ACS Sustainable Chem. Eng.* **2020**, *8*, 1644−1650.
(65) Shu, Y.; Lu, Q.; Yuan, F.; Tao, Q.; Jin, D.; Yao, H.; Xu, Q.; Hu, X. *ACS Appl. Mater. Interfaces* **2020**, 49480−49488.
(66) Chen, J.; Bao, J.; Cai, C.; Lu, T. *Anal. Chim. Acta* **2004**, *516*, 29−34.
(67) Malode, S. J.; Abbar, J. C.; Shetti, N. P.; Nandibewoor, S. T. *Electrochim. Acta* **2012**, *60*, 95−101.
(68) Medeiros, R. A.; Baccarin, M.; Fatibello-Filho, O.; Rocha-Filho, R. C.; Deslouis, C.; Debiemme-Chouvy, C. *Electrochim. Acta* **2016**, *197*, 179−185.
(69) Heidarimoghadam, R.; Farmany, A. *Mater. Sci. Eng., C* **2016**, *58*, 1242−1245.
(70) Zhao, D.; Wang, T.; Han, D.; Rusinek, C.; Steckl, A. J.; Heineman, W. R. *Anal. Chem.* **2015**, *87*, 9315−9321.
(71) Yue, W.; Riehl, B. L.; Pantelic, N.; Schlueter, K. T.; Johnson, J. M.; Wilson, R. A.; Guo, X.; King, E. E.; Heineman, W. R. *Electroanalysis* **2012**, *24*, 1039−1046.
(72) Christian, G. D.; Purdy, W. C. *J. Electroanal. Chem.* **1962**, *3*, 363−367.
(73) Hashemi, P.; Walsh, P. L.; Guillot, T. S.; Gras-Najjar, J.; Takmakov, P.; Crews, F. T.; Wightman, R. M. *ACS Chem. Neurosci.* **2011**, *2*, 658−666.
(74) Vonau, W.; Oelßner, W.; Guth, U.; Henze, J. *Sens. Actuators, B* **2010**, *144*, 368−373.
(75) Rius-Ruiz, F. X.; Kisiel, A.; Michalska, A.; Maksymiuk, K.; Riu, J.; Rius, F. X. *Anal. Bioanal. Chem.* **2011**, *399*, 3613−3622.
(76) Guth, U.; Gerlach, F.; Decker, M.; Oelßner, W.; Vonau, W. *J. Solid State Electrochem.* **2009**, *13*, 27−39.
(77) Kwon, N.-H.; Lee, K.-S.; Won, M.-S.; Shim, Y.-B. *Analyst* **2007**, *132*, 906.
(78) Shinwari, M. W.; Zhitomirsky, D.; Deen, I. A.; Selvaganapathy, P. R.; Deen, M. J.; Landheer, D. *Sensors* **2010**, *10*, 1679−1715.
(79) da Silva, E. T. S. G.; Miserere, S.; Kubota, L. T.; Merkoçi, A. *Anal. Chem.* **2014**, *86*, 10531−10534.
(80) Suzuki, H.; Hirakawa, T.; Sasaki, S.; Karube, I. *Anal. Chim. Acta* **1999**, *387*, 103−112.
(81) Matsumoto, T.; Ohashi, A.; Ito, N. *Anal. Chim. Acta* **2002**, *462*, 253−259.
(82) Bond, A. M.; Lay, P. A. *J. Electroanal. Chem. Interfacial Electrochem.* **1986**, *199*, 285−295.
(83) Pletcher, D. Why Microelectrodes?. In *Microelectrodes: Theory and Applications*; Springer Netherlands: Dordrecht, 1991; pp 3−16.
(84) Wang, Y.; Limon-Petersen, J. G.; Compton, R. G. *J. Electroanal. Chem.* **2011**, *652*, 13−17.
(85) Limon-Petersen, J. G.; Han, J. T.; Rees, N. V.; Dickinson, E. J. F.; Streeter, I.; Compton, R. G. *J. Phys. Chem. C* **2010**, *114*, 2227−2236.
(86) Musameh, M.; Wang, J.; Merkoci, A.; Lin, Y. *Electrochem. Commun.* **2002**, *4*, 743−746.
(87) Radoi, A.; Compagnone, D. *Bioelectrochemistry* **2009**, *76*, 126−134.
(88) Deng, C.; Chen, J.; Chen, X.; Xiao, C.; Nie, Z.; Yao, S. *Electrochem. Commun.* **2008**, *10*, 907−909.
(89) Moiroux, J.; Elving, P. J. *Anal. Chem.* **1978**, *50*, 1056−1062.
(90) Prieto-Simón, B.; Fàbregas, E. *Biosens. Bioelectron.* **2004**, *19*, 1131−1138.
(91) Wooten, M.; Gorski, W. *Anal. Chem.* **2010**, *82*, 1299−1304.
(92) Raj, C. R.; Chakraborty, S. *Biosens. Bioelectron.* **2006**, *22*, 700−706.
(93) Cadwallader, A. B.; De La Torre, X.; Tieri, A.; Botrè, F. *Br. J. Pharmacol.* **2010**, *161*, 1−16.
(94) Baranowska, I.; Markowski, P.; Gerle, A.; Baranowski, J. *Bioelectrochemistry* **2008**, *73*, 5−10.
(95) Semaan, F. S.; Pinto, E. M.; Cavalheiro, ÉT. G.; Brett, C. M. A. *Electroanalysis* **2008**, *20*, 2287−2293.
(96) Kor, K.; Zarei, K. *Talanta* **2016**, *146*, 181−187.
(97) Said, M. I.; Rageh, A. H.; Abdel-aal, F. A. M. *RSC Adv.* **2018**, *8*, 18698−18713.
(98) Wang, Y.; Cheng, J.; Liu, X.; Ding, F.; Zou, P.; Wang, X.; Zhao, Q.; Rao, H. *ACS Sustainable Chem. Eng.* **2018**, *6*, 16847−16858.
(99) Hasanzadeh, M.; Pournaghi-Azar, M. H.; Shadjou, N.; Jouyban, A. *RSC Adv.* **2014**, *4*, 6580.
(100) *WADA Technical Document-TD2019MRPL. WADA Technical Document-TD2019MRPL. WADA Technical Document-TD2019MRPL 2019. WADA Technical Document-TD2019MRPL.*
(101) Gupta, P.; Rahm, C. E.; Jiang, D.; Gupta, V. K.; Heineman, W. R.; Justin, G.; Alvarez, N. T. *Anal. Chim. Acta* **2021**, *1155*, No. 338353.

https://doi.org/10.1021/acs.analchem.1c00360
Anal. Chem. 2021, 93, 7439−7448